Inverse energy cascade in nonlocal helical shell models of turbulence

Massimo De Pietro,[1] Luca Biferale,[1] and Alexei A. Mailybaev[2]
[1]*Dip. di Fisica and INFN, Università "Tor Vergata," Via della Ricerca Scientifica 1, I-00133 Roma, Italy*
[2]*Instituto Nacional de Matemática Pura e Aplicada-IMPA, Est. Dona Castorina 110, Rio de Janeiro 22460-320 Brazil*
(Received 27 August 2015; published 28 October 2015)

Following the exact decomposition in eigenstates of helicity for the Navier-Stokes equations in Fourier space [F. Waleffe, Phys. Fluids A **4**, 350 (1992)], we introduce a modified version of helical shell models for turbulence with nonlocal triadic interactions. By using both an analytical argument and numerical simulation, we show that there exists a class of models, with a specific helical structure, that exhibits a statistically stable inverse energy cascade, in close analogy with that predicted for the Navier-Stokes equations restricted to the same helical interactions. We further support the idea that turbulent energy transfer is the result of a strong entanglement among triads possessing different transfer properties.

DOI: 10.1103/PhysRevE.92.043021 PACS number(s): 47.10.Fg, 47.27.ed

I. INTRODUCTION

Understanding and controlling the statistical and dynamical properties of turbulent flows is still an open problem in many fundamental and applied fields. From a theoretical point of view, the main difficulties stem from the highly nonlinear nature of the dynamics in the fully developed regime. Moreover, the presence of a large separation between the injection and dissipative scales and the empirical observation of non-Gaussian statistics of the velocity field make the system hard to approach with analytical perturbative techniques or brute force direct numerical simulations [1,2]. The physics of turbulent flow is very rich. It might depend on the embedding dimensionality, leading to a direct transfer of energy from large to small scales in three dimensions (forward cascade) or to an inverse transfer in two dimensions (backward cascade). Moreover, in the direct regime, turbulent flow develops anomalous scaling laws, where different moments of the velocity fluctuations possess a power-law behavior as a function of the separation scale, characterized by a set of anomalous scaling exponents.

For these reasons, many different techniques and approximations have been developed in order to try to better understand the turbulent phenomenology. One such approach is represented by shell models [3–11].

Shell models of turbulence are simplified models that mimic the Navier-Stokes (NS) equations in wave-number space. They are based on a strong reduction in the number of degrees of freedom, keeping only a few representative variables (typically one or two real variables) for the whole original set of wave numbers belonging to each shell. To have scaling invariance embedded in the system, the shell variables are defined on a set of wave numbers equally spaced on a logarithmic scale, $k_n \sim \lambda^n k_0$, where $\lambda = 2$ conventionally. In this way, a large separation of scales is achieved with relatively few variables. Furthermore, inspired by the Kolmogorov phenomenology for direct energy transfer, these models consider only local interactions in Fourier space, connecting dynamical evolution between three neighboring modes k_n, k_{n+1}, and k_{n+2}. Last but not least, the models are built in such a way that they have the same inviscid invariants of the original Navier-Stokes equations: energy and helicity for models of three-dimensional (3D) turbulence or energy and enstrophy for the 2D case.

Despite the huge simplifications, shell models share many properties with the original Navier-Stokes turbulence, including the development of anomalous scaling laws with values of scaling exponents very close to the ones measured in 3D turbulence [7–9,12]. Many generalizations to models for magnetohydrodynamics [13], rotating fluids [14–16], convection [17–21], and passive scalars [22–24] have also been studied.

Notwithstanding their success, shell models prove to be problematic when inverse energy cascade becomes the dominant phenomenon to be studied. In fact, in all known models for 2D turbulent flows that conserve energy and enstrophy, the inverse energy flux is overwhelmed by equilibrium fluctuations [25,26]. Similarly, also considering shell models of 3D Navier-Stokes equations restricted to having only sign-definite helicity [27], the inverse energy cascade is subleading with respect to equilibrium fluctuations [26]. Indeed, an inverse energy cascade in shell models has been observed only by adding extra terms in the equations of motion, representing mechanisms such as rotation or stratification [16,21], or considering the dynamics in a range of parameters where the conserved quantities have different physical dimensions with respect to those of the Navier-Stokes equations [26]. The main goal of this paper is to present a shell model that has energy and helicity as inviscid invariants, and that shows an inverse energy cascade without relying on any additional external mechanism beside the ones already present in the NS nonlinear term.

To better understand the interplay between helicity and energy, shell mmodels for 3D turbulence have been proposed in [28] using a close connection with the helical structure of the original Navier-Stokes equations. The idea was to apply the decomposition in helical eigenstates of the Navier-Stokes equations in order to distinguish triadic nonlinear interaction on the basis of their helical content [29]. It was indeed argued in [29] that depending on the relative sign of helicity carried by the three interacting modes, energy tends to be transferred forward or backward in 3D turbulent flow. Recently, further support for this statement was given in [27] by performing direct numerical simulations of 3D turbulence under the constraint of having only sign-definite helical modes and showing that in this case the flow inverts the energy transfer direction by pumping energy to larger and larger scales. As a result, clear evidence that inverse and direct energy

transfer mechanisms might coexist in 3D turbulence was given, making it even more interesting to understand under which circumstances the former prevails over the latter, or vice versa.

In this paper, we expand the work done in [28], trying to understand if the inclusion of helical variables in shell models might shed some light on the complexity of the energy transfer mechanism. In particular, we show that the *aspect ratio* of the triads is a key point. To achieve an inverse energy transfer mechanism, we relaxed the constraint of first-neighbor interactions between wave numbers. Indeed, we show, with both theoretical and numerical tools, that this simple modification can have dramatic consequences on the energy-cascade mechanism, turning a model that exhibits direct energy cascade into a model that exhibits an inverse energy cascade. It is remarkable that the argument suggesting the importance of elongated triads is taken in full similarity with the original case of 3D Navier-Stokes equations as developed originally in [29]: another case of a close overlap between the physics of turbulence and the dynamics of shell-models.

The paper is organized as follows. In Sec. II, the helical decomposition is briefly reviewed and a modified SABRA model with more *elongated* triads is defined. In Sec. III, predictions for the direction of the energy cascade and scaling laws are made on the basis of the stability analysis of a single interacting triad. In Sec. IV, results of numerical simulations are shown and compared with the predictions from the previous section. Finally, the two appendixes contain details and calculations. Appendix A contains the definition of a more general helical shell model with triads of any shape. Appendix B contains detailed calculations for the stability analysis of a single interacting triad.

II. HELICAL DECOMPOSITION FOR SHELL MODELS OF TURBULENCE

A. The original SABRA model

The original SABRA shell model [8] was inspired by the Navier-Stokes equations in Fourier space, and, although it cannot be formally derived from them, it has a phenomenology very similar to that of 3D homogeneous and isotropic turbulent flows. The model describes the evolution of a single complex variable u_n, representing all the modes in a shell of wave numbers $|\mathbf{k}| \in [k_n, k_{n+1}]$. The equations of motion take the form [8]

$$\dot{u}_n = i(ak_{n+1}u_{n+2}u^*_{n+1} + bk_n u_{n+1}u^*_{n-1} + ck_{n-1}u_{n-1}u_{n-2}) - \nu k_n^{\beta}u_n + f_n + \nu_l k_n^{-4}u_n, \quad (1)$$

where $k_n = k_0\lambda^n$, λ is an arbitrary scale parameter larger than unity (here $\lambda = 2$), νk_n^{β} is a dissipative ($\beta = 2$) or hyperdissipative ($\beta > 2$) term, f_n is an external forcing term, and $\nu_l k_n^{-4}$ is a large-scale damping term introduced for those models that develop an inverse energy transfer in order to get a stationary statistics. The model is defined on a given number of shells, $n = 0, 1, \ldots, N$, and the boundary conditions $u_{-1} = u_{-2} = u_{N+1} = u_{N+2} = 0$ are imposed.

The model has two quadratic inviscid invariants that depend on the values of the a, b, c parameters. The first one is always chosen to be the energy, $E = \sum_{n=0}^{N} |u_n|^2$, while the second can be defined to be unsigned to mimic helicity in 3D Navier-Stokes equations, $H = \sum_{n=0}^{N}(-)^n k_n |u_n|^2$, or positive definite as enstrophy for 2D NS, $\Omega = \sum_{n=0}^{N} k_n^2 |u_n|^2$. A significant drawback of the above model in the 3D regime is the imbalance between successive shell variables: the ones with an odd shell index carry only negative helical modes, while the ones with even n carry positive helicity [30–32].

B. The helical SABRA model

To overcome the previous limitation, a new class of shell models with a more realistic helicity structure was proposed in [28]. The first step was to follow the exact decomposition of the Navier-Stokes velocity field, in Fourier space, into positive and negative polarized helical waves [29]:

$$\mathbf{u}(\mathbf{x}) = \sum_{\mathbf{k}} (u^+_{\mathbf{k}}\mathbf{h}^+_{\mathbf{k}} + u^-_{\mathbf{k}}\mathbf{h}^-_{\mathbf{k}})e^{i\mathbf{k}\cdot\mathbf{x}}, \quad (2)$$

where $\mathbf{k}, \mathbf{h}^+_{\mathbf{k}}, \mathbf{h}^-_{\mathbf{k}}$ form an orthogonal basis, and the two $\mathbf{h}^s_{\mathbf{k}}$ (with $s = \pm$) are eigenvectors of the curl operator:

$$i\mathbf{k} \times \mathbf{h}^s_{\mathbf{k}} = sk\mathbf{h}^s_{\mathbf{k}}. \quad (3)$$

A possible way to construct them is to use the decomposition:

$$\mathbf{h}^s_{\mathbf{k}} = \boldsymbol{\nu}_{\mathbf{k}} \times \boldsymbol{\kappa} + is\boldsymbol{\nu}_{\mathbf{k}}, \quad (4)$$

where $\mathbf{k} = k\boldsymbol{\kappa}$, $\boldsymbol{\nu}_{\mathbf{k}} = (\mathbf{z} \times \boldsymbol{\kappa})/||\mathbf{z} \times \boldsymbol{\kappa}||$, and $\mathbf{z}$ is an arbitrary vector. The two fields $u^+_{\mathbf{k}}$ and $u^-_{\mathbf{k}}$ are merely the projections on the $\mathbf{h}^+_{\mathbf{k}}$ and $\mathbf{h}^-_{\mathbf{k}}$ directions of the Fourier coefficients of the velocity field, and they carry, respectively, positive and negative helicity. It was realized that by plugging this decomposition into the nonlinear term of the Navier-Stokes equations, one can distinguish eight possible nonlinear triadic interactions depending on the signs of the corresponding helical projections [29]. Four out of eight interactions are independent, because the interactions with reversed helicities are identical; they are summarized in Fig. 1. It is possible to apply the same decomposition verbatim to construct different classes of helical shell models with a more accurate helical structure than the original model (1). This first step was done in [28] introducing two complex variables u^+_n and u^-_n for every wave number, each one of them carrying positive or negative helicity and leading to the four independent classes of the local helical shell model. All of them have the form

$$\dot{u}^+_n = i\left(ak_{n+1}u^{s_1}_{n+2}u^{s_2*}_{n+1} + bk_n u^{s_3}_{n+1}u^{s_4*}_{n-1} + ck_{n-1}u^{s_5}_{n-1}u^{s_6}_{n-2}\right) - \nu k_n^{\beta}u^+_n + f^+_n - \nu_l k_n^{-4}u^+_n, \quad (5)$$

$$\dot{u}^-_n = i\left(ak_{n+1}u^{-s_1}_{n+2}u^{-s_2*}_{n+1} + bk_n u^{-s_3}_{n+1}u^{-s_4*}_{n-1} + ck_{n-1}u^{-s_5}_{n-1}u^{-s_6}_{n-2}\right) - \nu k_n^{\beta}u^-_n + f^-_n - \nu_l k_n^{-4}u^-_n, \quad (6)$$

where the helical indices $s_i = \pm$ are reported in Table I and the coefficients a, b, c can be found in Table II. Each one of these models evolves according to only one of the four independent helical interactions depicted in Fig. 1, where a triad (k_{n-1}, k_n, k_{n+1}) is represented by (k, p, q).

It is important to stress that, exactly as in the original Navier-Stokes equations, the four classes of interactions conserve energy and helicity separately if the coefficients a, b, c are chosen appropriately, i.e., they can be considered as four

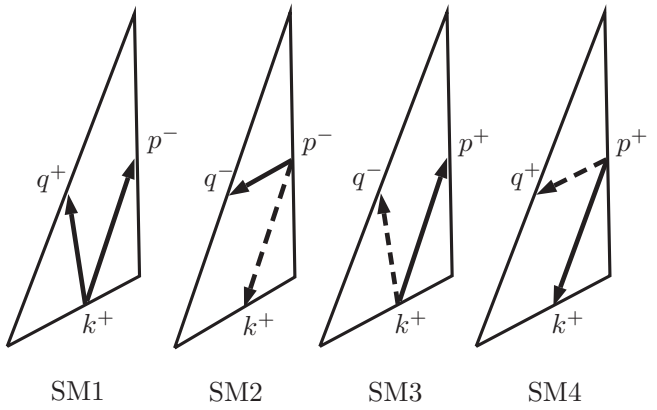

FIG. 1. Representation of the four independent classes of helical interaction between an ordered triad of wave numbers $k < p < q$, in both Navier-Stokes and helical shell models. The $\pm$ superscripts represent the helical mode, which is participating in the interaction. Each class has two possible interactions, which are equivalent due to the parity symmetry $k^+ \to k^-, p^+ \to p^-, q^+ \to q^-$; only one is shown here. The arrows represent the energy transfers, as a result of the instability assumption (see Sec. III and Appendix B). The dashed arrows represent weaker transfers with respect to the full lines. For models 1 and 3, energy flows out of the smallest wave number. In particular, in model 1, the smallest wave number transfers the same amount of energy to the other two, while model 3 exhibits a more localized energy transfer; in model 2, the middle wave number transfers more energy to the largest wave number and less to the smallest; and in model 4, the middle wave number transfers more energy to the smallest wave number and less to the largest.

submodels of the whole problem. The added value with respect to the previous SABRA structure is that now energy and helicity have the very same structure as for the NS equations [29] without the asymmetry among odd and even shells:

$$E = \sum_{n=0}^{N} (|u_n^+|^2 + |u_n^-|^2), \tag{7}$$

$$H = \sum_{n=0}^{N} k_n (|u_n^+|^2 - |u_n^-|^2). \tag{8}$$

As we shall see later, none of these four models is indeed able to show an inverse energy cascade. Even the shell model SM4, which is the equivalent of the Navier-Stokes restriction to sign-definite helical interactions [27], fails to develop an inverse energy transfer because of the presence of strong fluctuations due to the quasiequilibrium solution [26]. It is not surprising that the equilibrium solution might have a different

TABLE I. Helicity indices of Eqs. (5) and (6) and Eqs. (9) and (10) for the four models.

Model	s_1	s_2	s_3	s_4	s_5	s_6
SM1	+	−	−	−	−	+
SM2-SM2E	−	−	+	−	+	−
SM3	−	+	−	+	−	−
SM4	+	+	+	+	+	+

TABLE II. Coefficients of Eqs. (5) and (6) for the four helical shell models with first-neighbor interaction, plus the elongated version SM2E of model SM2 in Eqs. (9) and (10). These coefficients ensure energy and helicity conservation. Conventionally, and without loss of generality, we always choose $a = 1$.

Model	b	c
SM1	$-1/2$	$1/2$
SM2	$-5/2$	$-3/2$
SM2E	$-9/4$	$-5/4$
SM3	$-5/6$	$1/6$
SM4	$-3/2$	$-1/2$

influence on the shell model with respect to the Navier-Stokes equations, because of the strong difference in the scaling of the number of degrees of freedom as a function of the embedding physical dimension. *A priori* there is no reason why a very simplified structure such as the one given by shell models should replicate exactly the behavior of the Navier-Stokes equations restricted on the same helicity interactions class. In particular, one of the strongest limitations is given by the restriction to very local interactions among Fourier variables assumed by the structure (5).

In [29] it was shown, on the basis of an "instability assumption," that triads where the two highest wave numbers have the same helical sign, such as those in model SM2 (see Fig. 1), might lead to an inverse cascade. It was also explained that the key factor for the NS case is the triad geometry. Calling $v = k/p$ the ratio between the smallest and middle wave number, it was argued in [29], on the basis of a phenomenological scaling argument, that if $v < 0.278$, the triad should contribute to an inverse flux of energy, from small to large scales. In fact, empirical observation made on direct numerical simulations of the shell model SM2 (where $v = 0.5$) showed that energy flows toward small scales. We are therefore interested in extending the range of interactions, exploring smaller values of the ratio v, in order to meet the "elongation" requirement argued in [29].

C. The *elongated* helical SABRA model

We introduce here a shell model, which we will call SM2E, in which the triads are more elongated in the sense that the middle wave number k_n in a triad will interact with the first larger neighbor k_{n+1} and the second smaller neighbor k_{n-2}. In this way, we have the equivalent of the parameter $v = k_{n-2}/k_n = \lambda^{-2} = 0.25$ instead of $v = 0.5$ as for the local version. The model equations take the form

$$\dot{u}_n^+ = i\left(a k_{n+2} u_{n+3}^{s_1} u_{n+2}^{s_2 *} + b k_n u_{n+1}^{s_3} u_{n-2}^{s_4 *} + c k_{n-1} u_{n-1}^{s_5} u_{n-3}^{s_6}\right) - \nu k_n^{\beta} u_n^+ + f_n^+ - \nu_l k_n^{-4} u_n^+, \tag{9}$$

$$\dot{u}_n^- = i\left(a k_{n+2} u_{n+3}^{-s_1} u_{n+2}^{-s_2 *} + b k_n u_{n+1}^{-s_3} u_{n-2}^{-s_4 *} + c k_{n-1} u_{n-1}^{-s_5} u_{n-3}^{-s_6}\right) - \nu k_n^{\beta} u_n^- + f_n^- - \nu_l k_n^{-4} u_n^-, \tag{10}$$

where the helical indices s_i fall in the same helical class of the SM2 model (see Table I). The real constants a,b,c are determined by imposing that the triadic interaction conserves

energy (7) and helicity (8). The values of the resulting coefficients for the SM2E model are given in Table II. In Appendix A, we give the equations for an even more general shell model, allowing for interacting triads of any shape.

In the next section, we extend the "instability assumption" developed in [29] to predict the transfer properties of helical shell models, and we show that, indeed, the elongated version SM2E of the model SM2 should lead to an inverse energy transfer in agreement with the predictions for the set of triads with a similar geometrical factor in the Navier-Stokes equations.

III. ENERGY TRANSFERS IN HELICAL SHELL MODELS

In this section, we will first study the stability of steady states of only one triad of wave numbers. We will then extend the results of this analysis to a shell model with any number N of shells, in the framework of the instability assumption [29]. The instability assumption states two things: (i) the global statistical behavior of a shell model can be inferred directly from the single-triad dynamics; (ii) in a single-triad system, the energy flows from the most unstable wave number to the other two. Here the adjective "unstable" is intended to be used in the framework of the linear stability analysis of the equations for $u_n^{\pm}$. In fact, proceeding as in [29] and [28], we studied the linear stability of a single-triad helical shell model, both in its first-neighbor and elongated variants. This analysis (see Appendix B) confirms that there is one unstable wave number that transfers energy to the other two. For models SM1 and SM3 the unstable wave number is the smallest one, while for models SM2, SM2E, and SM4 the unstable wave number is the middle one (this property depends only on the helical class of the model, not on the triad shape). These results, already discussed in [28], are the same as those obtained for the Navier-Stokes equations, and they are summarized in Fig. 1.

A. Energy transfers

Let us now examine how one can exploit the stability analysis for a single triad to predict the sign of the energy transfer in a fully coupled shell model. For the balance of energy at shell k_n, we have

$$\dot{E}_n = \frac{d}{dt}(|u_n^+|^2 + |u_n^-|^2) = \left(\delta^E_{n+m} + b\delta^E_n - c\delta^E_{n-1}\right) - 2\nu k_n^{\beta} E_n + 2\,\mathrm{Re}(f^+ u_n^{+*} + f^- u_n^{-*}) - 2\nu_l k_n^{-4} E_n, \tag{11}$$

where

$$\delta^E_n = -2k_n \mathrm{Im}\left[\left(u^{s_3}_{n+1} u_n^{+*} u^{s_4 *}_{n-m}\right) + \left(u^{-s_3}_{n+1} u_n^{-*} u^{-s_4 *}_{n-m}\right)\right], \tag{12}$$

and $m = 1$ for the first-neighbor models SM1–SM4, or $m = 2$ for model SM2E. The total energy flux across a shell n is given by the balance equation

$$\sum_{j=0}^{n} \dot{E}_j = \Pi^E_n - \epsilon^{\mathrm{out}}_n + \epsilon^{\mathrm{in}}_n - \alpha^{\mathrm{out}}_n, \tag{13}$$

where the nonlinear contribution is given by $\Pi^E_n = \sum_{j=0}^{n}(\delta^E_{j+m} + b\delta^E_j - c\delta^E_{j-1})$, and with $\epsilon^{\mathrm{out}}_n = 2\nu \sum_{j=0}^{n} k_j^{\beta} E_j$ and $\alpha^{\mathrm{out}}_n = 2\nu_l \sum_{j=0}^{n} k_j^{-4} E_j$ we denote the dissipative contributions at small and large scales, respectively, while with $\epsilon^{in}_n = 2\sum_{j=0}^{n} \mathrm{Re}(f^+ u_j^{+*} + f^- u_j^{-*})$ we denote the external input from the forcing. Using the constraint of energy conservation $c = 1 + b$ (see Appendix A), one finds that the nonlinear contribution to the flux can be further simplified for models SM1–SM4 to

$$\Pi^E_n = (1+b)\delta^E_n + \delta^E_{n+1}, \tag{14}$$

while for model SM2E,

$$\Pi^E_n = (1+b)\delta^E_n + \delta^E_{n+1} + \delta^E_{n+2}. \tag{15}$$

The fact that the energy is conserved by the nonlinear terms implies that the nonlinear flux must vanish if calculated over all shells, $\Pi^E_N = 0$. In the presence of a stationary statistics, an average of the left-hand side of (13) must vanish too. For the case of a direct energy cascade ($\alpha^{\mathrm{out}}_N \sim 0$), the global energy balance imposes the equality of the time-averaged values $\langle \epsilon^{\mathrm{out}}_N \rangle = \langle \epsilon^{\mathrm{in}}_N \rangle$, while for the inverse energy cascade ($\epsilon^{\mathrm{out}}_N \sim 0$) we must have $\langle \alpha^{\mathrm{out}}_N \rangle = \langle \epsilon^{\mathrm{in}}_N \rangle$. In the presence of a direct cascade and in the inertial range of scales, i.e., for wave numbers k_n much larger than the forcing scales, k_f, and much smaller than the viscous scale, k_η, we must also have $\epsilon^{\mathrm{out}}_n = \alpha^{\mathrm{out}}_n \sim 0$ and $\langle \epsilon^{\mathrm{in}}_n \rangle = \mathrm{const}$. As a consequence, the existence of a constant direct energy cascade implies that $\langle \delta^E_n \rangle$ must be asymptotically constant (independent of n), such that also the flux will be constant and given by

$$\left\langle \Pi^E_n \right\rangle = f(b)\left\langle \delta^E_n \right\rangle = -\left\langle \epsilon^{in}_n \right\rangle = \mathrm{const}, \tag{16}$$

where $f(b) = (2 + b)$ for models SM1–SM4 and $f(b) = (3 + b)$ for model SM2E. Similarly, in the presence of an inverse energy cascade regime, for wave numbers k_n smaller than k_f we must have

$$\left\langle \Pi^E_n \right\rangle = f(b)\left\langle \delta^E_n \right\rangle = \left\langle \alpha^{\mathrm{out}}_n \right\rangle = \mathrm{const}. \tag{17}$$

In our notation, a negative flux means that energy is flowing from large to small scales and vice versa. The sign of $f(b)$ is known once a model is chosen, while for finding the sign of $\langle \delta^E_n \rangle$ we make use of the instability assumption as follows.

Given a one-triad model, considering only shells k_{n-m}, k_n, k_{n+1}, with zero energy injection and dissipation, Eq. (11), after averaging and under the hypothesis of constant flux, will take the form

$$\begin{aligned} \langle \dot{E}_{n-m} \rangle &= \langle \delta^E_n \rangle, \\ \langle \dot{E}_n \rangle &= b\langle \delta^E_n \rangle, \\ \langle \dot{E}_{n+1} \rangle &= -c\langle \delta^E_n \rangle. \end{aligned} \tag{18}$$

We can make several considerations based on Eq. (18). First, the ratio between the energies flowing toward the two stable wave numbers is simply given by the b and c coefficients of the model. Second, exploiting the instability assumption (Fig. 1), we can predict which wave number should have positive or negative energy variation (the unstable will have a negative energy derivative and vice versa); since b and c are known (Table II), the sign of $\langle \delta^E_n \rangle$ can be readily calculated. For instance, for model SM1, the mode with the smallest wave number is unstable, providing $\langle \dot{E}_{n-1} \rangle < 0$, $\langle \dot{E}_n \rangle > 0$ and $\langle \dot{E}_{n+1} \rangle > 0$; the values $b = -1/2 < 0$ and $c = 1/2 > 0$

TABLE III. Predictions for the energy flux, based on the instability assumption and Eqs. (13), (16), and (17). A negative energy flux means that energy is cascading toward small scales and vice versa. sgn[x] is the sign function.

Model	sgn[$\langle\delta_n^E\rangle$]	sgn[$f(b)$]	Energy flux prediction
SM1	−	+	Forward
SM2	+	−	Forward
SM2E	+	+	Backward
SM3	−	+	Forward
SM4	+	+	Backward

in Eq. (18) yield $\langle\delta_n^E\rangle < 0$. Similarly, for model SM3 we have $\langle\delta_n^E\rangle < 0$, while for models SM2 and SM4 $\langle\delta_n^E\rangle > 0$. These results do not depend on the triad shape, but only on the helical class of the interaction, so also for model SM2E $\langle\delta_n^E\rangle > 0$. From these calculations and Eq. (16) we derive the predictions for the direction of the energy flux given in Table III.

In this formalism, the information regarding the shape of the triad, i.e., the degree of nonlocality, is entirely contained in the $f(b)$ prefactor. To have a positive energy flux in Eq. (17), corresponding to an inverse energy cascade, the signs of the factors $\langle\delta_n^E\rangle$ and $f(b)$ must be the same. We see that the above argument predicts that model SM4 will have a positive energy flux and would be the first candidate for a shell model that displays inverse energy cascade. As shown in [26], it turns out that the fluctuations of the energy flux are so strong that such a system shows quasiequilibrium rather than an inverse cascade of energy. However, also switching from model SM2 to SM2E, the energy flux should reverse its sign, due to the sign change in the factor $f(b)$, as predicted also for the NS case. This provides a good candidate for a model with the same invariants as 3D Navier-Stokes equations exhibiting inverse energy cascade.

IV. NUMERICAL SIMULATIONS

To test the predictions made in Sec. III, and especially to see if the transition from the local shell model SM2 to the elongated shell model SM2E actually shows a reversal in the direction of the energy cascade, we have performed several numerical integrations of Eqs. (5) and (6) and Eqs. (9) and (10). The energy is injected through a stochastic Gaussian forcing, δ-correlated in time, with zero mean and $O(1)$ standard deviation on two shells, both on the positive (u_n^+) and negative (u_n^-) helicity-carrying velocities, with different amplitudes, in order to inject helicity as well. We performed several simulations, with energy injected at large, medium, or small scales, and for some of these cases we used hyperviscosity ($\sim k^4$ dissipative term) in order to have a cleaner inertial range without increasing too much the number of shells. We wanted to verify that this hyperviscosity does not have any important effect on the scaling laws of the observables. Also, a large-scale energy dissipation of the form $\sim k^{-4}$ was introduced in order to avoid large-scale energy accumulation where necessary. The parameters used for the simulations can be found in Table IV.

The time integration has been carried out using an explicit second-order Adams-Basforth scheme with exact integration

TABLE IV. Parameters used for the simulations. Several simulations were performed with energy injected at different shell numbers k_{n_f}. $|f_n^+|$ and $|f_n^+|$ represent the intensity (standard deviation) of the Gaussian forcing on the positive and negative helicity-carrying shells, respectively. Large-scale dissipation: $\nu_l k_n^{-4}$. Small-scale dissipation: sets I and II use a standard νk_n^2 viscosity, while sets III and IV use a νk_n^4 hyperviscosity. For all runs, $\lambda = 2$ and $k_0 = 1$.

	N	Δt	ν	ν_l	n_f	$\lvert f_n^+\rvert$	$\lvert f_n^-\rvert$
Run I	36	5×10^{-9}	1.0×10^{-12}	1	4,5	1	0.5
Run II	36	1×10^{-8}	1.0×10^{-12}	1	4,5	1	0.5
Run III	31	5×10^{-9}	2.5×10^{-28}	1	14,15	1	0.5
Run IV	31	1×10^{-8}	2.5×10^{-28}	1	22,23	1	0.5

of the viscous terms:

$$u_n(t+\Delta t) = u_n(t)e^{-\gamma_n \Delta t} + \Delta t\left[\frac{3}{2}e^{-\gamma_n \Delta t}NLT_n(t) - \frac{1}{2}e^{-2\gamma_n \Delta t}NLT_n(t-\Delta t)\right], \tag{19}$$

where γ_n and NLT_n are, respectively, the viscous and the nonlinear terms on the right-hand side of Eqs. (5) and (6) or Eqs. (9) and (10). The stochastic forcing is integrated separately with a forward Euler scheme.

The equations were evolved for several hundreds of large-scale eddy turnover times, T_e, and time averages were first calculated on runs lasting $T \sim 10T_e$ and then averaged again over all the stationary runs. Stationarity is checked by monitoring the total energy evolution. Figures 2 and 3 show the energy spectra for the local SM2 and elongated SM2E models, for both large-scale and small-scale energy injection cases. Figure 4 shows the corresponding energy flux for the case when the forcing mechanism is acting at an intermediate scale, such as to resolve simultaneously the forward and backward transfers. We briefly remind the reader that in terms of shell-model variables, a forward/backward energy cascade

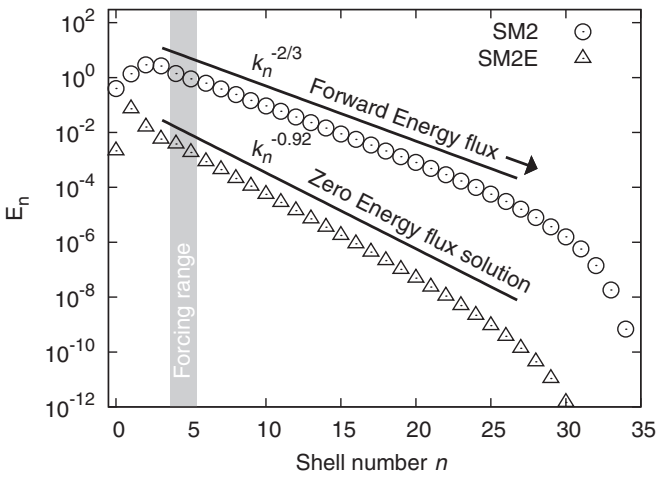

FIG. 2. Energy spectra E_n for the two variants of model 2, forced at large scales (gray-shaded region). Curves are shifted vertically for clarity. Parameters used for this simulation are in Table IV (runs I and II).

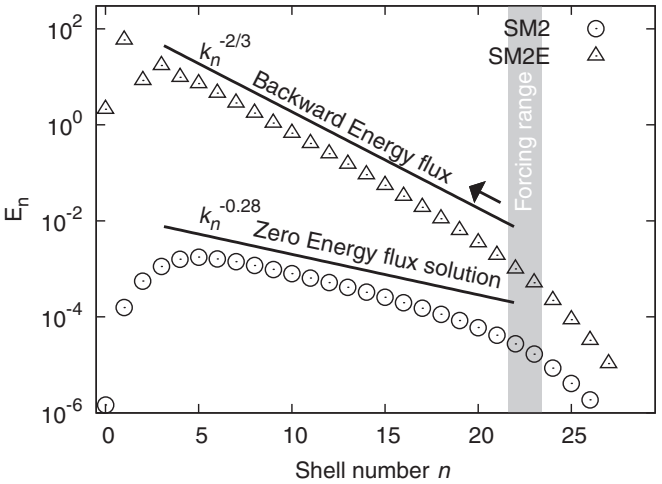

FIG. 3. Energy spectra E_n for the two variants of model 2, forced at small scales (gray-shaded region). Curves are shifted vertically for clarity. Parameters used for this simulation are in Table IV (run IV).

gives the scaling $E_n \sim |\epsilon|^{2/3}k^{-2/3}$, while a dynamics close to energy equipartition should give $E_n \sim$ const.

From Figs. 2 and 4 we clearly see that model SM2 has a forward energy transfer and no backward transfer. On the other hand, Figs. 3 and 4 show that model SM2E has the opposite behavior: a clear backward energy transfer and zero forward flux. Let us further notice that in the regime where the energy flux is absent, both models do not develop a solution close to energy equipartition. Indeed, in these ranges the dynamics can be dominated by a homogeneous solution of the energy balance equation (11) in the stationary regime. In fact, by substituting the definitions (14) or (15) inside the stationary balance equation for the flux, $\langle \Pi_n^E \rangle = \epsilon$, where the sign of ϵ depends on whether we have a forward or a backward cascade, we obtain the following for the two models SM2 and SM2E:

$$(1+b)\langle \delta_n^E \rangle + \langle \delta_{n+1}^E \rangle = \epsilon \qquad \text{(SM2)}, \tag{20}$$

$$(1+b)\langle \delta_n^E \rangle + \langle \delta_{n+1}^E \rangle + \langle \delta_{n+2}^E \rangle = \epsilon \qquad \text{(SM2E)}. \tag{21}$$

The solution of these difference equations is generally a sum of the solution of the corresponding homogeneous equation (zero-flux solution, or *zero mode*) and a particular solution, for instance $\langle \delta_n^E \rangle = \text{const}$, that represents the constant flux solution [33]. If the homogeneous solution has a steeper scaling than the constant-flux solutions, it is subdominant in the dynamics. On the other hand, when the constant energy flux solution is absent, the homogeneous zero mode may become dominant. This explains the slope of the energy spectrum for the SM2 model in the range $k < k_f$, where a direct calculation shows that the dynamics is dominated by a zero-mode solution of (20), $\langle \delta_{n+1}^E \rangle / \langle \delta_n^E \rangle = -(1+b) = \lambda^{0.585}$, leading to the scaling law $|u_n|^2 \sim (\langle \delta_n^E \rangle / k_n)^{2/3} \sim k_n^{0.277}$; see Fig. 3. The same may also happen with the SM2E model in the range $k > k_f$, where the scaling imposed by the zero mode, $|u_n|^2 \sim k_n^{-0.92}$, is very close to that observed in Fig. 2.

For completeness, we must say that there are situations in which the scaling dictated by the zero mode of the energy flux is the same as the scaling given by the constant helicity flux solution. Also, the zero mode of the helicity flux may dictate the same scaling as that given by the constant energy flux solution. This happens for models SM1 and SM4.

Another interesting question is about intermittency. It is generally believed that inverse cascades do not show any anomalous scaling, i.e., they are not intermittent, while forward cascades do. One way of quantifying intermittency is by looking at the flatness, the ratio between the fourth-order moment and the squared second-order moment, as a function of the reference scale. Figure 5 shows the flatness of the total

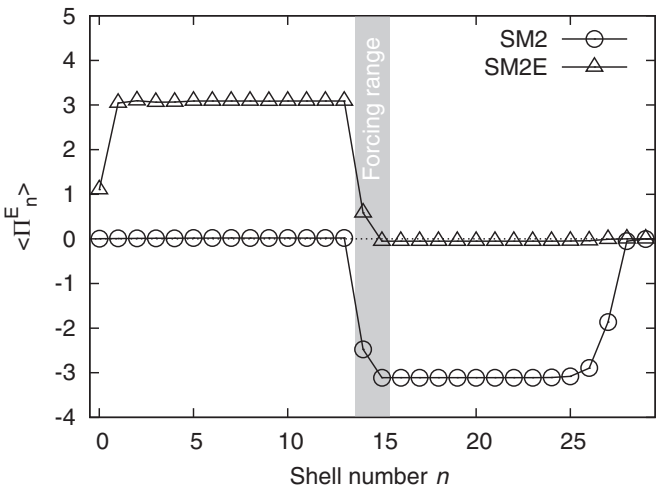

FIG. 4. Energy flux $\langle \Pi_n^E \rangle$ for the two variants of model 2, forced at medium scales (gray-shaded region). We recall that, with our notation, a positive energy flux corresponds to an inverse cascade of energy, and vice versa. Parameters used for this simulation are in Table IV (run III).

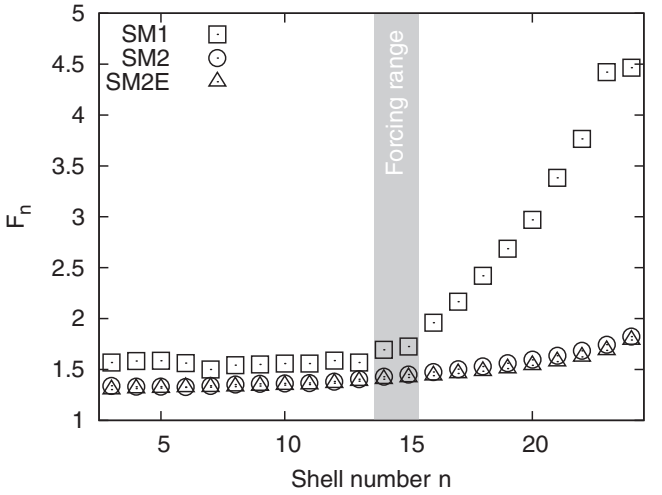

FIG. 5. Flatness F_n for models SM1, SM2, and SM2E, forced at medium scales (gray-shaded region). Model SM1 is intermittent in the $n > n_f$ range. Models SM2 and SM2E show a very weak level of intermittency for $n > n_f$. Parameters used for this simulation are in Table IV (run III).

shell energy defined as

$$F_n = \frac{S_4(k_n)}{[S_2(k_n)]^2} \tag{22}$$

for models SM1, SM2, and SM2E, where the structure functions $S_q(k_n)$ are defined in terms of the energy flux (14) and (15):

$$S_q(k_n) = \left\langle \left(k_n^{-1} \left| \Pi_n^E \right| \right)^{\frac{q}{3}} \right\rangle. \tag{23}$$

The larger the values of the flatness, the more non-Gaussian is the PDF. As one can see, model SM1 develops a clear anomalous scaling in the forward regime (for $k_n > k_f$) and no intermittency for $k < k_f$, where it is known to be dominated by equilibrium statistics (no backward energy transfer). Note that model SM1 can be shown to be equivalent to the original SABRA model, which is known to have an intermittent dynamics in the $n > n_f$ range. Models SM2 and SM2E have very little visible deviations in the forward regimes and no intermittency at all in the backward regime, in agreement with the observation that inverse cascades do not develop anomalous scaling [34,35]. These results are generally interpreted in term of the hierarchy of time scales in the system: a forward energy cascade with spectrum $E_n \sim k_n^{-2/3}$ implies that the typical eddy turnover time at shell n goes like $\tau_n \sim 1/(k_n u_n) \sim k_n^{-2/3}$, i.e., energy is transferred to faster and faster modes, preventing small scales to equilibrate around the mean properties of the large ones. On the other hand, an inverse energy cascade with the same slope is dominated by exactly the opposite dynamics, i.e., fast scales transfer fluctuations to slower ones allowing for self-averaging. It is not clear if this phenomenology is at the root also of shell-models dynamics, where energy is known to be transferred also via quasi-instantonic solutions traveling coherently among a huge set of shell variables [36–40]. This argument is the aim of a work in progress, and it will be reported elsewhere.

Finally, for models having helical interaction SM2, in order to check that the reversal in the energy flux is robust when the ratio of the smallest to the middle wave number is $v < 0.278$ [29], we simulated numerically another model, with first-neighbor and third-neighbor interactions (k_{n-3},k_n,k_{n+1}) (see Appendix A). For this model, $v = 0.125$, and the results for the energy spectrum, the energy fluxes, and the intermittency are qualitatively the same as for the model SM2E (not shown).

V. CONCLUSIONS

We have generalized a previously proposed class of helical shell models to include also nonlocal triadic interactions among Fourier modes. Using arguments similar to those developed for the Navier-Stokes equations [29], we have shown that a suitable subset of helical triadic interactions may change the energy transfer direction depending on the relative geometry of the three interacting modes, leading to direct or inverse cascades. We also show that the inverse cascade is not intermittent and that the scaling properties in the range of shells where the energy does not flow might be dominated by a zero-mode solution of the energy balance equations. This work paves the way to studying the coupling between different models with different helical interactions and triad shapes in order to understand and mimic those transitions from direct to inverse cascades observed in real flows upon changing the degree of rotation, aspect ratio, or large scale shear [41,42]. Coupling models with different transfer properties makes it more challenging to disentangle the effects of the dynamics coming from each single model. Schemes such as mode-to-mode energy transfer [43,44] can be efficiently combined with our formalism to address this issue. Another interesting direction for future work is to understand the influence of high helicity content on the dynamics of direct and inverse triadic interactions, or, in general, the dynamics of the helicity in the inverse cascade model, as was done in [32] for the direct cascade model SM3.

ACKNOWLEDGMENTS

M.D.P. and L.B. acknowledge funding from the European Research Council under the European Union's Seventh Framework Programme, ERC AdG NewTURB Agreement No 339032. A.A.M. was supported by the CNPq (Grant No. 305519/2012-3) and by the FAPERJ (Pensa Rio 2014).

APPENDIX A: EQUATIONS AND COEFFICIENTS FOR A HELICAL SABRA SHELL MODEL WITH GENERIC WAVE-NUMBER TRIADS

In this Appendix, we present the equations for a SABRA shell model with a generic triad shape. For the sake of simplicity, we omit the forcing and the dissipative terms. The equations are

$$\begin{aligned} \frac{d}{dt}u_n^+ &= i\big(ak_{n+m}u_{n+m+l}^{s_1}u_{n+m}^{s_2*} + bk_n u_{n+l}^{s_3}u_{n-m}^{s_4*} \\ &\quad + ck_{n-l}u_{n-l}^{s_5}u_{n-m-l}^{s_6}\big), \\ \frac{d}{dt}u_n^- &= i\big(ak_{n+m}u_{n+m+l}^{-s_1}u_{n+m}^{-s_2*} + bk_n u_{n+l}^{-s_3}u_{n-m}^{-s_4*} \\ &\quad + ck_{n-l}u_{n-l}^{-s_5}u_{n-m-l}^{-s_6}\big). \end{aligned} \tag{A1}$$

Here a,b,c are real coefficients, the helical indices $s_i = \pm$ are reported in Table I, and the triad shape (k_{n-m},k_n,k_{n+l}) is described by the pair of indices m and l. The coefficient a can always be set equal to 1 just by rescaling the other coefficients and time. The coefficients b and c are fixed by imposing the conservation of the quadratic inviscid invariants as follows.

It can be shown that Eq. (A1) admit only four quadratic inviscid invariants. Only two out of the four can be simultaneously conserved, due to the fact that there are only two free parameters (b and c). The four possible invariants are as follows:

(i) $W^{\mathrm{I}} \equiv \sum_n k_n^{\alpha_I}(|u^+|^2 + |u^-|^2)$, which for $\alpha_{\mathrm{I}} = 0$ corresponds to the total energy.

(ii) $W^{\mathrm{II}} \equiv \sum_n k_n^{\alpha_{\mathrm{II}}}(|u^+|^2 - |u^-|^2)$, which is not sign-definite and for $\alpha_{\mathrm{II}} = 1$ corresponds to the total helicity.

(iii) $W^{\mathrm{III}} \equiv \sum_n (-1)^n k_n^{\alpha_{\mathrm{III}}}(|u^+|^2 + |u^-|^2)$.

(iv) $W^{\mathrm{IV}} \equiv \sum_n (-1)^n k_n^{\alpha_{\mathrm{IV}}}(|u^+|^2 - |u^-|^2)$.

Only W^{I} and W^{II} have the same physical meaning as the invariants of the NS equations, while for W^{III} and W^{IV} there is no such analogy.

TABLE V. General expression for the coefficients of Eq. (A1) conserving generic invariants W^{I} and W^{II}. Without loss of generality, $a = 1$. For models that conserve energy and helicity, one should set $\alpha_{\mathrm{I}} = 0$ and $\alpha_{\mathrm{II}} = 1$.

Model	b	c
1	$\frac{\lambda^{\alpha_{\mathrm{I}}(m+l)}[1-\lambda^{(m+l)(\alpha_{\mathrm{II}}-\alpha_{\mathrm{I}})}]}{\lambda^{m(\alpha_{\mathrm{I}}+\alpha_{\mathrm{II}})}(\lambda^{l\alpha_{\mathrm{II}}}+\lambda^{l\alpha_{\mathrm{I}}})}$	$-\frac{\lambda^{m\alpha_{\mathrm{I}}}[-1-\lambda^{m(\alpha_{\mathrm{II}}-\alpha_{\mathrm{I}})}]}{\lambda^{m(\alpha_{\mathrm{I}}+\alpha_{\mathrm{II}})}(\lambda^{l\alpha_{\mathrm{II}}}+\lambda^{l\alpha_{\mathrm{I}}})}$
2	$\frac{\lambda^{\alpha_{\mathrm{I}}(m+l)}[-1-\lambda^{(m+l)(\alpha_{\mathrm{II}}-\alpha_{\mathrm{I}})}]}{\lambda^{m(\alpha_{\mathrm{I}}+\alpha_{\mathrm{II}})}(\lambda^{l\alpha_{\mathrm{II}}}-\lambda^{l\alpha_{\mathrm{I}}})}$	$\frac{\lambda^{m\alpha_{\mathrm{I}}}[-1-\lambda^{m(\alpha_{\mathrm{II}}-\alpha_{\mathrm{I}})}]}{\lambda^{m(\alpha_{\mathrm{I}}+\alpha_{\mathrm{II}})}(\lambda^{l\alpha_{\mathrm{II}}}-\lambda^{l\alpha_{\mathrm{I}}})}$
3	$\frac{\lambda^{\alpha_{\mathrm{I}}(m+l)}[-1-\lambda^{(m+l)(\alpha_{\mathrm{II}}-\alpha_{\mathrm{I}})}]}{\lambda^{m(\alpha_{\mathrm{I}}+\alpha_{\mathrm{II}})}(\lambda^{l\alpha_{\mathrm{II}}}+\lambda^{l\alpha_{\mathrm{I}}})}$	$\frac{\lambda^{m\alpha_{\mathrm{I}}}[-1+\lambda^{m(\alpha_{\mathrm{II}}-\alpha_{\mathrm{I}})}]}{\lambda^{m(\alpha_{\mathrm{I}}+\alpha_{\mathrm{II}})}(\lambda^{l\alpha_{\mathrm{II}}}+\lambda^{l\alpha_{\mathrm{I}}})}$
4	$\frac{\lambda^{\alpha_{\mathrm{I}}(m+l)}[-1+\lambda^{(m+l)(\alpha_{\mathrm{II}}-\alpha_{\mathrm{I}})}]}{\lambda^{m(\alpha_{\mathrm{I}}+\alpha_{\mathrm{II}})}(-\lambda^{l\alpha_{\mathrm{II}}}+\lambda^{l\alpha_{\mathrm{I}}})}$	$\frac{\lambda^{m\alpha_{\mathrm{I}}}[-1+\lambda^{m(\alpha_{\mathrm{II}}-\alpha_{\mathrm{I}})}]}{\lambda^{m(\alpha_{\mathrm{I}}+\alpha_{\mathrm{II}})}(-\lambda^{l\alpha_{\mathrm{II}}}+\lambda^{l\alpha_{\mathrm{I}}})}$

The triad-by-triad conservation of a W^{I}-type invariant implies

$$0 = \frac{d}{dt}\sum_n k_n^{\alpha}(|u_n^+|^2 + |u_n^-|^2) = \sum_n k_n^{\alpha}(\dot{u}_n^+ u_n^{+*} + \dot{u}_n^- u_n^{-*} + \text{c.c.}), \tag{A2}$$

where all the terms on the right-hand side must formally cancel for each triad after substituting Eq. (A1). For all four classes of helical interaction, the resulting conservation equation is

$$a + \lambda^{\alpha_{\mathrm{I}} m} b - \lambda^{\alpha_{\mathrm{I}}(m+l)} c = 0. \tag{A3}$$

The conservation of a W^{II}-type invariant yields, respectively,

$$a - \lambda^{\alpha_{\mathrm{II}} m} b - \lambda^{\alpha_{\mathrm{II}}(m+l)} c = 0 \quad \text{(SM1)}, \tag{A4}$$

$$a - \lambda^{\alpha_{\mathrm{II}} m} b + \lambda^{\alpha_{\mathrm{II}}(m+l)} c = 0 \quad \text{(SM2)}, \tag{A5}$$

$$a + \lambda^{\alpha_{\mathrm{II}} m} b + \lambda^{\alpha_{\mathrm{II}}(m+l)} c = 0 \quad \text{(SM3)}, \tag{A6}$$

$$a + \lambda^{\alpha_{\mathrm{II}} m} b - \lambda^{\alpha_{\mathrm{II}}(m+l)} c = 0 \quad \text{(SM4)}. \tag{A7}$$

As mentioned before, we can always choose $a = 1$. Solving Eqs. (A3) and (A4)–(A7) for each model, we get the generic expressions for the b and c coefficients, which are reported in Table V.

APPENDIX B: INSTABILITY ASSUMPTION

For completeness, we repeat here the calculations done in [28] for the linear stability analysis of a triad of interacting wave numbers. Let us consider a system made of three consecutive wave numbers k_1, $k_2 = \lambda k_1$, and $k_3 = \lambda^2 k_1$ ($\lambda > 1$), and, for instance, model SM1. The equations of motion (5) and (6) for such a system reduce to

$$\begin{aligned} \dot{u}_1^+ &= ik_2 a u_3^+ u_2^{-*}, \\ \dot{u}_2^- &= ik_2 b u_3^+ u_1^{+*}, \\ \dot{u}_3^+ &= ik_2 c u_2^- u_1^+. \end{aligned} \tag{B1}$$

This system has three equilibrium states, of the form $(u_1^+, u_2^-, u_3^+) \in \{(A,0,0);(0,A,0);(0,0,A)\}$, where $A \in \mathbb{C}$. Linearization of the system around a generic state ($u_n^s \to u_n^s + \Delta_n^s$, with $\Delta_n^s \ll 1$) gives

$$\begin{aligned} \dot{\Delta}_1^+ &= ik_2 a(\Delta_2^{-*} u_3^+ + \Delta_3^+ u_2^{-*}), \\ \dot{\Delta}_2^- &= ik_2 b(\Delta_1^{+*} u_3^+ + \Delta_3^+ u_1^{+*}), \\ \dot{\Delta}_3^+ &= ik_2 c(\Delta_1^+ u_2^- + \Delta_2^- u_1^+). \end{aligned} \tag{B2}$$

The eigenvalues relative to the first state $(A,0,0)$ are

$$\lambda_1 = 0\,, \quad \lambda_{2,3} = \pm k_2 |A| \sqrt{-bc} = \pm k_2 |A|/2, \tag{B3}$$

where we substituted $-bc = 1/4$ (see Table II), hence the equilibrium state is unstable because one of the perturbations grows exponentially in time as $\Delta_i \sim \exp(k_2|A|t/2)$.

Similarly, the eigenvalues relative to the second state $(0,A,0)$ are

$$\lambda_1 = 0\,, \quad \lambda_{2,3} = \pm k_2 |A| \sqrt{-ac} = \pm i k_2 |A|/\sqrt{2}, \tag{B4}$$

so all the perturbations Δ_i are bounded in time. The same can be said for the third state $(0,0,A)$, for which the eigenvalues are

$$\lambda_1 = 0\,, \quad \lambda_{2,3} = \pm k_2 |A| \sqrt{ab} = \pm i k_2 |A|/\sqrt{2}. \tag{B5}$$

According to the terminology of [29], a wave-number k_1 represented by the unstable equilibrium state $(A,0,0)$, where the energy is flowing toward the other modes k_2 and k_3, is called unstable. Similarly, wave numbers k_2 and k_3 are stable with respect to small perturbations, as suggested by (B4) and (B5). So we see that for model SM1, the unstable wave number is the smallest one. Furthermore, the stability depends only on the sign of the coefficients a,b,c, which again depends only on the type of helical interaction chosen, while the triad shape does not play any role. In fact, repeating the same calculations with a different triad shape gives exactly the same stability results.

Analogous equations can be written for the other models, and it is found that for model SM3 the unstable wave number is the smallest one, while for models SM2, SM2E, and SM4 the unstable wave number is the middle one, as summarized in Fig. 1.

[1] S. B. Pope, *Turbulent Flows* (Cambridge University Press, Cambridge, 2000).
[2] U. Frisch, *Turbulence: The Legacy of A. N. Kolmogorov* (Cambridge University Press, Cambridge, 1995).
[3] A. Obukhov, Some general characteristic equations of the dynamics of the atmosphere, Izvestiya Akad. Nauk SSSR, Fiz. Atmos. Okeana **7**, 695 (1971).
[4] E. B. Gledzer, System of hydrodynamic type admitting two quadratic integrals of motion, Sov. Phys. Dokl. **18**, 216 (1973).
[5] V. N. Desnianskii and E. A. Novikov, Evolution of turbulence spectra toward a similarity regime, Akad. Nauk SSSR, Izv., Fiz. Atmo. Okeana **10**, 127 (1974).

[6] M. Yamada and K. Ohkitani, The inertial subrange and non-positive Lyapunov exponents in fully-developed turbulence, Prog. Theor. Phys. **79**, 1265 (1988).

[7] M. H. Jensen, G. Paladin, and A. Vulpiani, Intermittency in a cascade model for three-dimensional turbulence, Phys. Rev. A **43**, 798 (1991).

[8] V. S. L'vov, E. Podivilov, A. Pomyalov, I. Procaccia, and D. Vandembroucq, Improved shell model of turbulence, Phys. Rev. E **58**, 1811 (1998).

[9] L. Biferale, Shell models of energy cascade in turbulence, Annu. Rev. Fluid Mech. **35**, 441 (2003).

[10] T. Bohr, M. H. Jensen, G. Paladin, and A. Vulpiani, *Dynamical Systems Approach to Turbulence* (Cambridge University Press, Cambridge, 2005).

[11] P. D. Ditlevsen, *Turbulence and Shell Models* (Cambridge University Press, Cambridge, 2010).

[12] D. Pisarenko, L. Biferale, D. Courvoisier, U. Frisch, and M. Vergassola, Further results on multifractality in shell models, Phys. Fluids A **5**, 2533 (1993).

[13] F. Plunian, R. Stepanov, and P. Frick, Shell models of magneto-hydrodynamic turbulence, Phys. Rep. **523**, 1 (2013).

[14] M. Reshetnyak and B. Steffen, The shell model approach to the rotating turbulence, arXiv:physics/0311001.

[15] Y. Hattori, R. Rubinstein, and A. Ishizawa, Shell model for rotating turbulence, Phys. Rev. E **70**, 046311 (2004).

[16] S. Chakraborty, M. H. Jensen, and A. Sarkar, On two-dimensionalization of three-dimensional turbulence in shell models, Eur. Phys. J. B **73**, 447 (2010).

[17] A. Brandenburg, Energy Spectra in a Model for Convective Turbulence, Phys. Rev. Lett. **69**, 605 (1992).

[18] J. Mingshun and L. Shida, Scaling behavior of velocity and temperature in a shell model for thermal convective turbulence, Phys. Rev. E **56**, 441 (1997).

[19] E. S. C. Ching and W. C. Cheng, Anomalous scaling and refined similarity of an active scalar in a shell model of homogeneous turbulent convection, Phys. Rev. E **77**, 015303 (2008).

[20] E. S. C. Ching, H. Guo, and T. S. Lo, Refined similarity hypotheses in shell models of homogeneous turbulence and turbulent convection, Phys. Rev. E **78**, 026303 (2008).

[21] A. Kumar and M. K. Verma, Shell model for buoyancy-driven turbulence, Phys. Rev. E **91**, 043014 (2015).

[22] M. H. Jensen, G. Paladin, and A. Vulpiani, Shell model for turbulent advection of passive-scalar fields, Phys. Rev. A **45**, 7214 (1992).

[23] R. Benzi, L. Biferale, and A. Wirth, Analytic Calculation of Anomalous Scaling in Random Shell Models for a Passive Scalar, Phys. Rev. Lett. **78**, 4926 (1997).

[24] I. Arad, L. Biferale, A. Celani, I. Procaccia, and M. Vergassola, Statistical Conservation Laws in Turbulent Transport, Phys. Rev. Lett. **87**, 164502 (2001).

[25] E. Aurell, G. Boffetta, A. Crisanti, P. Frick, G. Paladin, and A. Vulpiani, Statistical mechanics of shell models for two-dimensional turbulence, Phys. Rev. E **50**, 4705 (1994).

[26] T. Gilbert, V. S. L'vov, A. Pomyalov, and I. Procaccia, Inverse Cascade Regime in Shell Models of Two-Dimensional Turbulence, Phys. Rev. Lett. **89**, 074501 (2002).

[27] L. Biferale, S. Musacchio, and F. Toschi, Inverse Energy Cascade in Three-Dimensional Isotropic Turbulence, Phys. Rev. Lett. **108**, 164501 (2012).

[28] R. Benzi, L. Biferale, R. M. Kerr, and E. Trovatore, Helical shell models for three-dimensional turbulence, Phys. Rev. E **53**, 3541 (1996).

[29] F. Waleffe, The nature of triad interactions in homogeneous turbulence, Phys. Fluids A **4**, 350 (1992).

[30] P. D. Ditlevsen and P. Giuliani, Cascades in helical turbulence, Phys. Rev. E **63**, 036304 (2001).

[31] Q. Chen, S. Chen, and G. L. Eyink, The joint cascade of energy and helicity in three-dimensional turbulence, Phys. Fluids **15**, 361 (2003).

[32] T. Lessinnes, F. Plunian, R. Stepanov, and D. Carati, Dissipation scales of kinetic helicities in turbulence, Phys. Fluids **23**, 035108 (2011).

[33] C. M. Bender and S. A. Orszag, *Advanced Mathematical Methods for Scientists and Engineers*, International Series in Pure and Applied Mathematics (McGrew–Hill, New York, 1978).

[34] J. Paret and P. Tabeling, Intermittency in the two-dimensional inverse cascade of energy: Experimental observations, Phys. Fluids **10**, 3126 (1998).

[35] G. Boffetta, A. Celani, and M. Vergassola, Inverse energy cascade in two-dimensional turbulence: Deviations from gaussian behavior, Phys. Rev. E **61**, R29 (2000).

[36] T. Dombre and J. L. Gilson, Intermittency, chaos and singular fluctuations in the mixed Obukhov-Novikov shell model of turbulence, Physica D **111**, 265 (1998).

[37] L. Biferale, G. Boffetta, A. Celani, and F. Toschi, Multi-time, multi-scale correlation functions in turbulence and in turbulent models, Physica D **127**, 187 (1999).

[38] I. Daumont, T. Dombre, and J. L. Gilson, Instanton calculus in shell models of turbulence, Phys. Rev. E **62**, 3592 (2000).

[39] P. Constantin, B. Levant, and E. S. Titi, Regularity of inviscid shell models of turbulence, Phys. Rev. E **75**, 016304 (2007).

[40] A. A. Mailybaev, Blowup as a driving mechanism of turbulence in shell models, Phys. Rev. E **87**, 053011 (2013).

[41] P. J. Staplehurst, P. A. Davidson, and S. B. Dalziel, Structure formation in homogeneous freely decaying rotating turbulence, J. Fluid Mech. **598**, 81 (2008).

[42] H. Kellay and W. I. Goldburg, Two-dimensional turbulence: A review of some recent experiments, Rep. Prog. Phys. **65**, 845 (2002).

[43] G. Dar, M. K. Verma, and V. Eswaran, Energy transfer in two-dimensional magnetohydrodynamic turbulence: Formalism and numerical results, Physica D **157**, 207 (2001).

[44] M. K. Verma, Statistical theory of magnetohydrodynamic turbulence: Recent results, Phys. Rep. **401**, 229 (2004).